Natural Radioactivity in Select Serpentinite-Related Nephrite Samples: A Comparison with Dolomite-Related Nephrite

Dariusz Malczewski, Michał Sachanbiński, and Maria Dziurowicz

The published literature offers only a few records of direct measurement of the natural radioactivity in nephrite. The present study used high-purity germanium (HPGe) low-background gamma-ray spectrometry to measure activity concentrations of primordial radionuclides in 11 serpentinite-related nephrite (ortho-nephrite) samples from deposits in Poland, Russia, Canada, and New Zealand, along with three samples of rodingite and serpentinite from a nephrite deposit in Nasławice, Poland. All nephrite samples exhibited very low ^{40}K, ^{232}Th, and ^{238}U activity concentrations that fell within the range of published values for ultrabasic and basic rocks. The nephrite samples from Jordanów (Poland) gave the highest uranium and thorium activity concentration values. Two samples of plagiogranitic rodingite showed significantly higher ^{238}U and ^{232}Th activity concentrations than the values measured for nephrite. Nephrite thorium and uranium concentrations correlated strongly (r = 0.98), and the corresponding Th/U ratios appear unique according to geographical location. The mean estimated potassium, thorium, and uranium concentrations from ortho-nephrite analyzed here were compared with corresponding mean values previously reported for dolomite-related nephrite (para-nephrite). The comparison indicates that the ortho-nephrites studied have similar uranium concentrations but lower mean potassium concentrations and higher mean thorium concentrations than those reported for para-nephrite in the literature.

Nephrite jade is an almost monomineral rock made of full-grained (felted), cryptocrystalline amphiboles (actinolite and tremolite) (Łoboś et al., 2008; Adamo and Bocchio, 2013; Gil et al., 2020; Gao et al., 2020). Nephrite usually appears green with varying degrees of saturation but may also exhibit white, gray, black, yellow, brown, and red coloration (Luo et al., 2015; Gil et al., 2020). In most cases, the color of nephrite is influenced by Cr^{3+}, Fe^{2+}, and Fe^{3+} ions that produce a wide range of light to dark green hues (Suturin et al., 1980; Hobbs, 1982). The intensity of the green coloration is mainly a function of the total iron content (Wilkins et al., 2003; Grapes and Yun, 2010). This sometimes creates mottled, striped, or veined varieties with marbled patterns.

See end of article for About the Authors and Acknowledgments.
Gems & Gemology, Vol. 58, No. 2, pp. 196–213,
http://dx.doi.org/10.5741/GEMS.58.2.196

Nephrite's internal structure typically appears fibrous, with an intricately woven microstructure of thin tremolite filaments and microtubules that form kidney-like shapes. The name "nephrite" thus derives from the Greek word for kidney (Łoboś et al., 2008). It is characterized by a high degree of compactness and coherence as well as extreme compressive strength. One nephrite from British Columbia, Canada, exhibited a fracture strength of about 200 MN m^{-2} (Makepeace and Simandl, 2001). By contrast, nephrite has a hardness of approximately 6.5 on the Mohs scale. The specific gravity of nephrite usually ranges between 2.90 and 3.06 (Żaba, 2006). The main global economic deposits of nephrite jade occur in Canada, Russia, China, the United States, South Korea, New Zealand, Australia, Poland, Italy, and Switzerland. These are usually classified as:

1. Endogenic deposits formed as a result of geological processes of internal origin. The origin of these deposits relates to serpentinites

(ortho-nephrite, serpentinite-related nephrite) and dolomites (para-nephrite, dolomite-related nephrite).

2. Exogenic deposits representing secondary placer deposits of nephrite blocks associated with river and stream sediments, for instance, in East Sayan (Russia), New Zealand, and British Columbia (Canada).

This study measured the radioactivity concentration of ^{40}K, ^{232}Th, and ^{238}U in ortho-nephrite samples from five known nephrite deposits using gamma-ray spectrometry. A major goal of this research was to ascertain whether, as valued decorative stones and gemstones, nephrite may pose a radiological risk to those who handle them, such as artisans or collectors. The authors also sought to compare Th/U ratios of ortho- and para-nephrite. As a secondary goal, the research sought evidence that Th/U concentration ratios vary with the geographic origin of nephrite. The results were compared with limited data available from previous studies on samples from the same localities. Previously published data consist primarily of potassium concentrations but also include thorium and uranium concentrations reported for para-nephrite and obtained by other analytical methods (Leaming, 1978; Łoboś et al., 2008; Grapes and Yun, 2010; Burtseva et al., 2015; Gil et al., 2015).

Dolomite-related nephrite forms at the contact between dolomite marble and a granitic intrusion or siliceous metasediments (Nichol, 2000; Yui and Kwon, 2002; Gil et al., 2015). Different formation processes cause ortho-nephrite and para-nephrite to vary in terms of their concentrations of transition metals and trace elements. Due primarily to lower iron and chromium concentrations, para-nephrite displays lighter colors ranging from white to light green (Luo et al., 2015). Ratios of iron to magnesium and concentrations of chromium, nickel, cobalt, and manganese distinguish para-nephrite from ortho-nephrite. Along with trace element concentrations, hydrogen and oxygen stable isotopic ratios have been used to determine the geographic origin of select dolomite-related nephrite deposits (Gao et al., 2020). As many concentrations of minor elements overlap for both types of nephrite, expanding the range of trace element determinations and overall geochemical datasets could refine models and criteria for distinguishing dolomite-related and serpentinite-related nephrite. Expanded geochemical datasets also offer greater accuracy and precision to studies of nephrite provenance.

Consensus holds that ortho-nephrite forms due to initial rodingitization and subsequent serpentinite transformation under the influence of gabbroic or acid magma injection (Gil et al., 2015). Genetic relations between these phases and associated rock types thus warranted investigation of both serpentinite and rodingite that co-occur at the Nasławice locality.

In Brief

- Gamma-ray measurements indicate very low ^{40}K, ^{232}Th, and ^{238}U activity concentrations in 11 serpentinite-related (ortho-nephrite) samples.
- Two samples of plagiogranitic rodingite from a nephrite deposit in Nasławice (Poland) showed significantly higher ^{238}U and ^{232}Th activity concentrations than those measured for nephrite samples.
- Thorium and uranium concentrations correlate positively and linearly in the ortho-nephrites analyzed.
- Nephrite, a valued decorative stone and gemstone, does not pose a radiological risk to artisans or collectors.

MATERIALS AND METHODS

This study analyzed samples of gem-quality ortho-nephrite originating from Poland (Nasławice, Jordanów), Russia (Siberia, East Sayan), Canada (British Columbia), and New Zealand (South Island). Polished nephrite samples referred to as NS1, NS2, and NS3 (table 1 and figure 1, A–C) were collected by M. Sachanbiński from an active serpentinite and nephrite quarry in Nasławice (Łoboś et al., 2008).

Raw jade samples referred to as JR1, JR2, and JR3 (table 1 and figure 1, D–F) belong to the collection of M. Sachanbiński and come from the historic jade quarry in Jordanów (Prichystal, 2013). Nephrite in Nasławice and nearby Jordanów occurs in serpentinite of the Gogołów-Jordanów Massif (GJM), which forms part of the Ślęża Ophiolite, itself part of the Mid-Sudetic Ophiolite (Gil, 2013; Gil et al., 2020). These nephrites occur as irregular bodies within the so-called black wall, a chlorite body within a contact zone of rodingite dikes and serpentinite. The serpentinites in Jordanów and Nasławice host completely transformed gabbro and plagiogranites as well as partially rodingitized leucogranites. Nephrite from Jordanów and Nasławice is considered of high gemological quality and usually appears green but without uniform coloration. Varied shades of green create unique patterns on the material's surface.

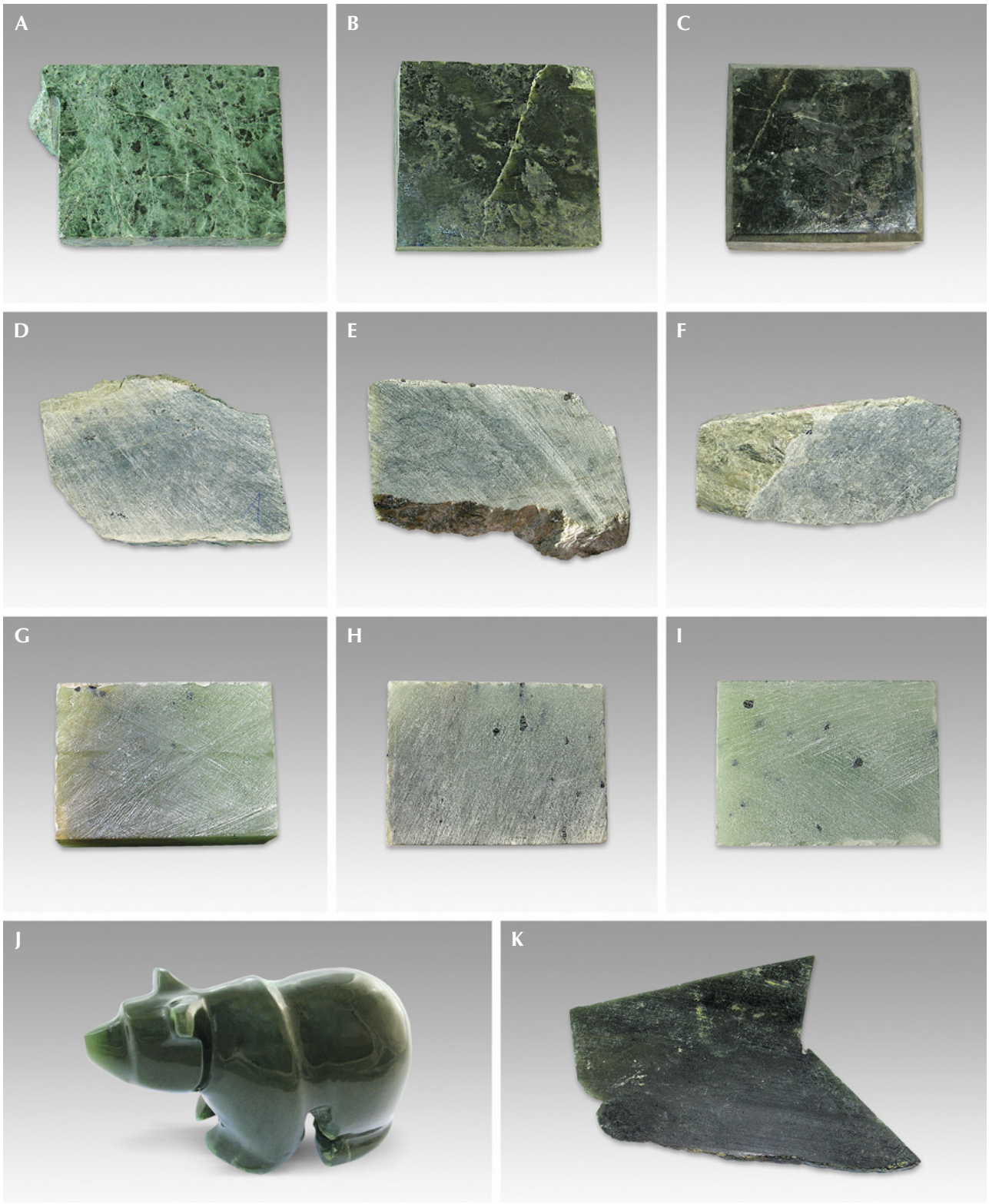

Figure 1. Photographs of ortho-nephrite samples analyzed. A: From Nasławice (NS1), 7 cm in length. B: From Nasławice (NS2), 7 cm in length. C: From Nasławice (NS3), 3 cm in length. D: From Jordanów (JR1), 4 cm in length. E: From Jordanów (JR2), 4 cm in length. F: From Jordanów (JR3), 4 cm in length. G: From Siberia (SB1), 3 cm in length. H: From Siberia (SB2), 3 cm in length. I: From Siberia (SB3), 3 cm in length. J: Bear carving from British Columbia (CN1), 7 cm in length. K: From New Zealand (NZ1), ~7 cm across. All photos by D. Malczewski.

Actinolite represents the main mineral comprising nephrite, and secondary minerals include chlorite, antigorite, grossular, chromite, and iron oxides.

Russian nephrite samples SB1, SB2, and SB3 (table 1 and figure 1, G–I) belong to the collection of M. Sachanbiński. These were donated by a Russian geologist during the International Mineralogical Association conference in Novosibirsk, Russia, in September 1978. The samples come from the Ospa deposit located in the East Sayan nephrite-bearing area (southern folded periphery of the Siberian craton). This deposit represents an apo-ultrabasic nephrite (Burtseva et al., 2015). Nephrite from the deposit appears greenish blue in color and exhibits different degrees of saturation (Suturin et al., 1980). Mineral compositions consist primarily of actinolite and tremolite fibers, pyroxene, diopside, serpentine, talc, chromite, graphite, and fuchsite. Accessory mineral content ranges from 0.5 to 1.5%. All of the above-mentioned nephrite samples from Nasławice and Jordanów (Poland) and Siberia (Russia) will be donated to the Mineralogical Museum of the University of Wrocław (Poland).

Canadian sample CN1 is a dark green nephrite carved in the form of a small bear (table 1 and figure 1J). This carving also belongs to the collection of M. Sachanbiński and was purchased during the 17th General Meeting of the IMA in Toronto in August 1998. It was made by a First Nations artisan using material from British Columbia, where more than 50 nephrite occurrences have been reported. These consist of individual blocks, talus blocks, boulder fields, and *in situ* bodies that occur primarily at contacts between serpentinite and cherts, or other metasedimentary and igneous rocks formed in submarine environments. Secondary minerals in the nephrite include spinel, diopside, uvarovite, titanite, chlorite, and talc (Leaming, 1978; Makepeace and Simandl, 2001).

Nephrite sample NZ1 from the South Island of New Zealand exhibits a waxy luster and blackish green color (table 1, figure 1K). This sample was donated to the Mineralogical Museum at the Institute of Earth Sciences, University of Silesia by L. Sajkowski, a Polish geologist living and working in New Zealand. Grapes and Yun (2010) describe this nephrite from northern Westland as occurring as rare pebbles and boulders weighing up to several tons, found in glacial outwash gravels and till. They also appear in streams and rivers that drain the nephrite source area of the *pounamu* ultramafic rocks located in the northern part of the Southern Alps (Ireland et al., 1984; Cooper, 1995).

Samples RN1, RN2, and RN3 represent rodingite (table 1). Rodingite is a rare type of metasomatic rock consisting of grossular, diallage, and accessory magnetite, apatite, and serpentinized olivine. It can be enriched in epidote, prehnite, and vesuvianite (Bell et al., 1911; O'Brien and Rodgers, 1973; Hatzipanagiotou and Tsikouras, 2001; Kobayashi and Kaneda, 2010; Heflik et al., 2014). The samples and rock type are considered to have high ornamental value. The analyzed samples belong to the collection of S. Madej from the University of Wrocław and come from an active serpentinite and jade quarry in Nasławice. Dubińska et al. (2004) distinguish two types of rodingite. The first type, boninite rodingite, contains relict clinopyroxene and vesuvianite, garnet, and diopside. The second type, plagiogranite rodingite, contains relics of checkerboard albite and hydrogrossular, clinozoisite, zoisite, and late diopside. Macroscopically, samples RN1 and RN2 (plagiogranite rodingites; figure 2, A and B) exhibit alternating, fine-grained, light and pink-colored laminae and medium-grained, dark gray laminae. In their study of the phase compositions of this type of rodingite, Szełęg (2006) reported quartz (approx. 63%), zoisite (approx. 25%), carbonate-hydroxyl apatite, hydrogrossular, albite, and smaller amounts of apatite, titanite, chromite, uraninite, and thorianite. Sample RN3 (boninite rodingite) (figure 2C) exhibits dull to light green color and varied mineral composition.

Sample SRN (table 1, figure 2D) belongs to the collection of M. Sachanbiński and represents a typical serpentinite from the deposit in Nasławice. Serpentinites occurring there formed as a result of complex, long-term transformation of harzburgite and lherzolite (Dubińska and Gunia, 1997). These belong to the Gogołów-Jordanów Serpentinite Massif of the Ślęża Ophiolite and probably formed at around 400 Ma (million years ago) (Gil et al., 2015). The serpentinite from Nasławice appears dark green in color and consists primarily of antigorite and sometimes contains olivine, bronzite, diallage, diopside, and hornblende. They sometimes resemble nephrite or are nephritized to varying degrees. Subordinate minerals include magnesite, braunite, chromite, apatite, garnet, and others. Macroscopically, these minerals are prized for their decorative value. The use of serpentinite as tools or decorative objects dates back to the Neolithic (around 3000 BCE) in Lower Silesia. The stone was originally used in tools and weapons (e.g., axes, knives, and hoes) and is used today in ornamental objects (see box A).

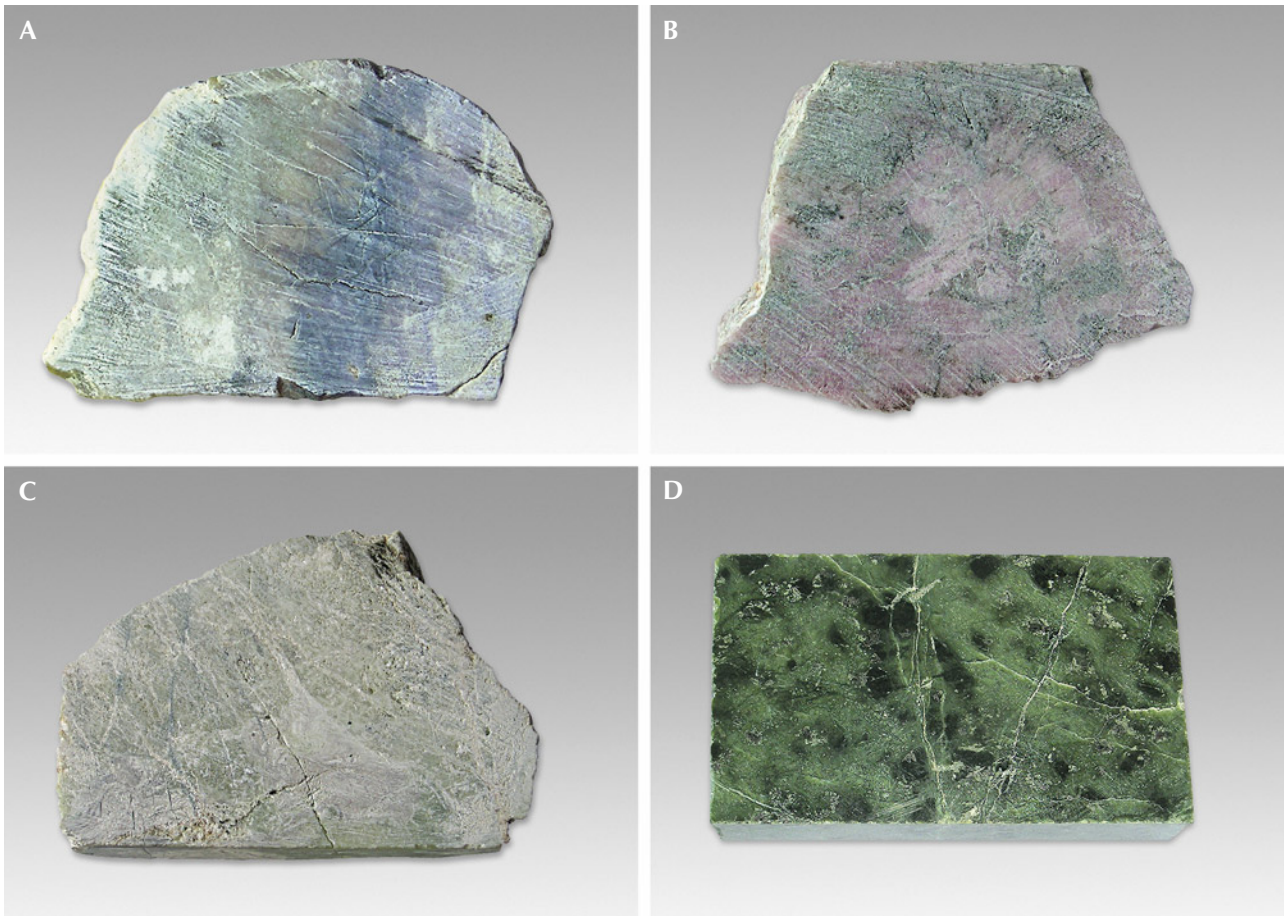

Figure 2. Samples of rodingite and serpentinite from Nasławice. A: Plagiogranitic rodingite (RN1), 4 cm in length. B: Plagiogranitic rodingite (RN2), 6 cm in length. C: Boninitic rodingite (RN3), 6.5 cm in length. D: Serpentinite (SRN), 6 cm in length. All photos by D. Malczewski.

The activity concentrations (in Bq kg^{-1}) of the naturally occurring radionuclides in nephrite, rodingite, and serpentinite samples, shown in table 1, were measured using a GX4018 gamma-ray spectrometry

Box A: Use of Nephrite Jade

The practical and ornamental use of nephrite jade by humans dates back to at least the early Neolithic. Because its fracture yields sharp, durable edges, nephrite was initially used to make axes, knives, scrapers, and other simple cutting tools. A pile deposit discovered along the shores of Lake Constance, Switzerland, contained 30,000 jade axes weighing a total of 6000 kg (Hobbs, 1982; Prichystal, 2013). A younger Stone Age site near Jordanów (Jordansmuhl) in Lower Silesia, Poland, is interpreted as a serpentinite and nephrite mining and processing center (Prichystal, 2013). A block of jade weighing over two tons excavated from the Jordanów site in 1889 was on display in the New York Metropolitan Museum of Art (Gil, 2013).

Jade continues to be used for ornamental and decorative objects such as jewelry and art. Some of the highest-quality nephrite, referred to as *pounamu* in the Maori language, is mined in New Zealand (Hobbs, 1982; Prichystal, 2013). The Maori utilized jade for ornaments, art, and tools—in the latter case until the introduction of metal in the nineteenth century. Chinese culture and artwork have featured jade since its earliest inception, and jade carving is particularly well developed in East Asia (Douglas, 2005; Wang, 2011). Nephrite jade has been considered a symbol of wealth and power, and thus many jade artifacts have survived intact into modern times. From antiquity to the present day, nephrite jade has been considered a store of value and items made from it have been prized as gifts.

TABLE 1. Measured radionuclide activity concentrations and calculated weight concentrations of ^{40}K, ^{232}Th, and ^{238}U from ortho-nephrite, rodingite, and serpentinite samples.[a]

	^{40}K		^{232}Th		^{238}U	
Rock/Sample	Bq kg^{-1}	Total K wt.%[b]	Bq kg^{-1}	ppm	Bq kg^{-1}	ppm
Nephrite						
NS1	1.5	0.005	0.5	0.12	1.6	0.13
NS2	1.2	0.004	0.6	0.15	1.8	0.15
NS3	5.5	0.018	2.0	0.49	4.5	0.36
JR1	17	0.055	4.4	1.08	19	1.34
JR2	13	0.042	4.7	1.16	20	1.62
JR3	14	0.045	4.3	1.06	17	1.38
SB1	5.1	0.016	1.9	0.47	6.2	0.50
SB2	6.8	0.022	2.0	0.49	5.9	0.48
SB3	5.1	0.016	1.9	0.47	6.6	0.53
CN1	27	0.087	0.8	0.20	1.2	0.10
NZ1	4.2	0.014	1.5	0.37	1.3	0.11
Rodingite						
RN1	14	0.045	130	32.0	292	23.6
RN2	28	0.091	18	4.43	172	13.9
RN3	2.7	0.009	4.6	1.13	10	0.81
Serpentinite						
SRN	1	0.003	0.7	0.17	1.1	0.09

[a]*Measurement uncertainties are plotted with this data in figures 4–7.*
[b]*The following conversion factors were used: K (wt.%) = ^{40}K (Bq kg^{-1})/309.11; Th (ppm) = ^{232}Th (Bq kg^{-1})/4.06; and U (ppm) = ^{238}U (Bq kg^{-1})/12.35 (International Atomic Energy Agency, 2003). Uncertainties fell within 5–10% of measured values for activity concentrations below 2 Bq kg^{-1}.*

system at the Laboratory of Natural Radioactivity, Institute of Earth Sciences, University of Silesia (Malczewski et al., 2018a, 2018b; see also box B). The system uses a high-purity germanium (HPGe) detector (45.2% efficiency) in a lead and copper shield (10.2 cm) with a multichannel-buffer Lynx instrument. The energy resolutions of the detector were 0.8 keV at 122 keV and 1.7 keV at 1330 keV. Each sample was

analyzed for 96 h. The activity concentrations of ^{232}Th and ^{238}U were determined based on the gamma-ray activity concentrations of ^{208}Tl, ^{212}Pb, and ^{228}Ac for thorium, and ^{214}Pb and ^{214}Bi for uranium. Radionuclide activity concentrations were calculated from the following gamma-ray transitions (energy in keV): ^{40}K (1460.8); ^{208}Tl (583.1, 860.5, 2614.5); ^{212}Pb (238.6, 300.1); ^{214}Pb (242, 295.2, 351.9); ^{214}Bi (609.3, 1120.3, 1764.5); and ^{228}Ac (338.32, 911.6, 964.6, 969.1). Laboratory Sourceless Calibration Software (LabSOCS) and Genie 2000 v.3.4 software packages were both used to analyze spectra, calibrate efficiency, and determine radionuclides.

Consistency of the activity concentrations calculated for gamma-ray transitions for a given multiline radionuclide (e.g., ^{208}Tl, ^{214}Bi, ^{214}Pb, and ^{228}Ac) were checked using line activity consistency evaluator (LACE) analysis. For all measurements, the multiline radionuclides gave activity concentration ratios approaching unity. The average minimum detectable activity concentration (MDA) for measured radionuclides was 0.1 Bq kg^{-1}. Figure 3 shows examples of gamma-ray spectra for nephrite samples NS1 and JR1 and rodingite sample RN1.

RESULTS AND DISCUSSION

Table 1 lists measured activity concentrations for ^{40}K, ^{232}Th, and ^{238}U in Bq kg^{-1} and calculated potassium (wt.%), thorium (ppm), and uranium (ppm) concentrations for nephrite, rodingite, and serpentinite samples.

^{40}K. As seen in figure 4 and table 1, the ^{40}K activity concentrations recorded for nephrite samples analyzed ranged from 1.2 Bq kg^{-1} for NS2 to 27 Bq kg^{-1} for CN1. Nephrite from Nasławice, Jordanów, and Siberia gave average values of 2.7, 15, and 5.7 Bq kg^{-1}, respectively. The New Zealand nephrite (NZ1) had an intermediate value of 4.2 Bq kg^{-1}. The average value for all samples was 9.1 Bq kg^{-1} (figure 4). These values exceed ^{40}K ac-

BOX B: NATURAL RADIOACTIVITY

Natural radioactivity results from the spontaneous decay of naturally occurring radioisotopes. All elements having an atomic number greater than 83 consist only of radioactive isotopes. The three natural types of radioactive nuclei decay include alpha (α, emission of helium nuclei), beta (β, emission of electrons or positrons), and gamma (γ, emission of the shortest electromagnetic waves) decay. The SI unit of radioactivity is the becquerel (Bq), equal to one decay per second. The becquerel replaced the curie (Ci), the unit equal to 3.7×10^{10} disintegrations per second or the radioactivity of 1 g of ^{226}Ra (1 Bq = 0.27×10^{-10} Ci). The main source of radioactivity in minerals, rocks, and soils derives from the ^{232}Th, ^{235}U, ^{238}U decay series, and ^{40}K (non-series). The ^{232}Th, ^{235}U, and ^{238}U series consist of 6 α and 4 β, 7 α and 4 β, and 8 α and 6 β decays, respectively. Many of the α and β decays are accompanied by gamma-ray radiation. The major gamma transitions from potassium, thorium, and uranium are commonly used in estimating weight concentrations based on measured activity concentrations. Due to the low natural abundance of ^{235}U (0.72% of natural uranium), the activity concentration of this isotope is usually negligible compared to that of ^{238}U. Its activity concentration is thus not taken into account.

Typical soils and carbonate rocks give average ^{40}K, ^{232}Th, and ^{238}U activity concentrations of 400, 30, and 35 Bq kg^{-1} and 80, 7, and 27 Bq kg^{-1}, respectively (Van Schmus, 1995; UNSCEAR, 2000). Among the most common rock types, acidic igneous rocks such as granite and rhyolite give the highest radioactivity values. These typically range from 900–1400, 50–200, and 37–72 Bq kg^{-1} for ^{40}K, ^{232}Th, and ^{238}U, respectively.

The activity concentration index assesses radiological hazards to human health posed by building materials, including rock surfaces used in paneling or countertops. The European Union standard index I, as defined by the European Atomic Energy Community (2013), represents the sum of three isotopic fractions expressed as:

$$I = \frac{A_{Ra}}{300\ \text{Bq kg}^{-1}} + \frac{A_{Th}}{200\ \text{Bq kg}^{-1}} + \frac{A_K}{3000\ \text{Bq kg}^{-1}}$$

where A_{Ra}, A_{Th}, and A_K represent ^{226}Ra (^{238}U), ^{232}Th, and ^{40}K (Bq kg^{-1}) activity concentrations in surroundings or material. The value of index I should not exceed unity, which corresponds to the indoor dose rate of 1 mSv y^{-1}. The sievert (Sv) is the SI unit of equivalent dose and effective dose equal to 1 J kg^{-1}. The external hazard index H_{ex} is also commonly used to evaluate the radiological risk of building materials. It is calculated as follows:

$$H_{ex} = \frac{A_{Ra}}{370\ \text{Bq kg}^{-1}} + \frac{A_{Th}}{259\ \text{Bq kg}^{-1}} + \frac{A_K}{4810\ \text{Bq kg}^{-1}}$$

An H_{ex} index equal to unity corresponds to an external gamma-ray dose of 1.5 mSv y^{-1} from a material. With a few exceptions, the overwhelming majority of rock building materials are characterized by I and H_{ex} values less than one. All ortho-nephrites measured in this study have extremely low average I and H_{ex} values of 0.04 and 0.03, respectively.

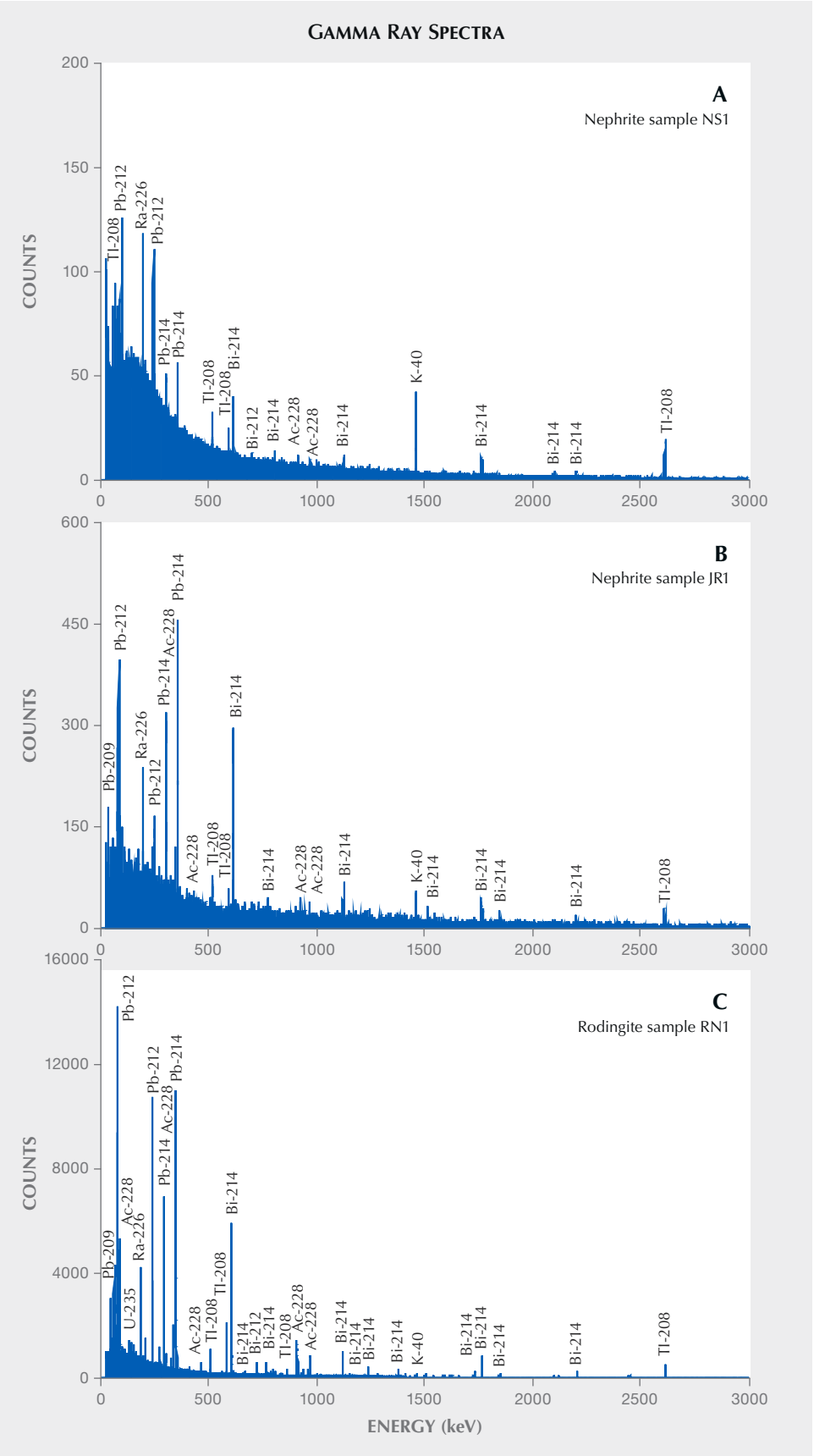

Figure 3. Gamma-ray spectra from nephrite sample NS1 (A), nephrite sample JR1 (B), and rodingite sample RN1 (C). Characteristic gamma-ray emitters are marked above the corresponding peaks. Note the different y-axis count scales for the three samples.

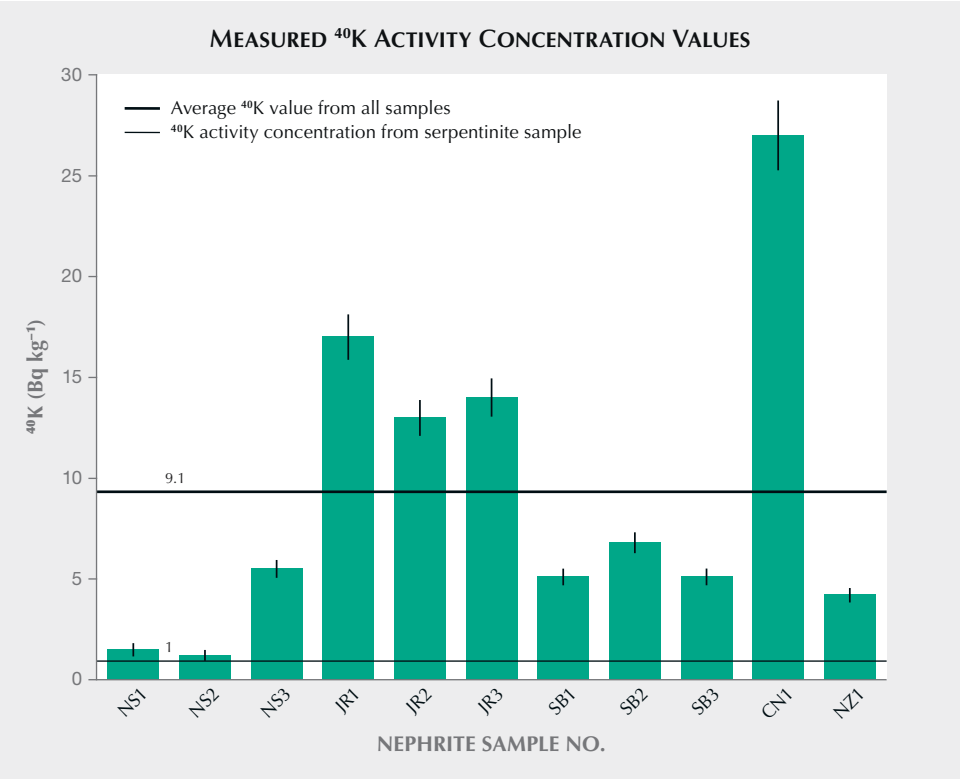

Figure 4. Measured ^{40}K activity concentration values. The thick horizontal line represents the average ^{40}K value measured from all samples in this study. The thin horizontal line represents the ^{40}K activity concentration for the serpentinite sample (SRN). The thin vertical lines are error bars.

tivity concentration values estimated from ultramafic rocks (~ 0.3 Bq kg^{-1}; Van Schmus, 1995) and serpentinite (1 Bq kg^{-1}) but fell below average values measured in gabbros from Lower Silesia (73 Bq kg^{-1}; Plewa and

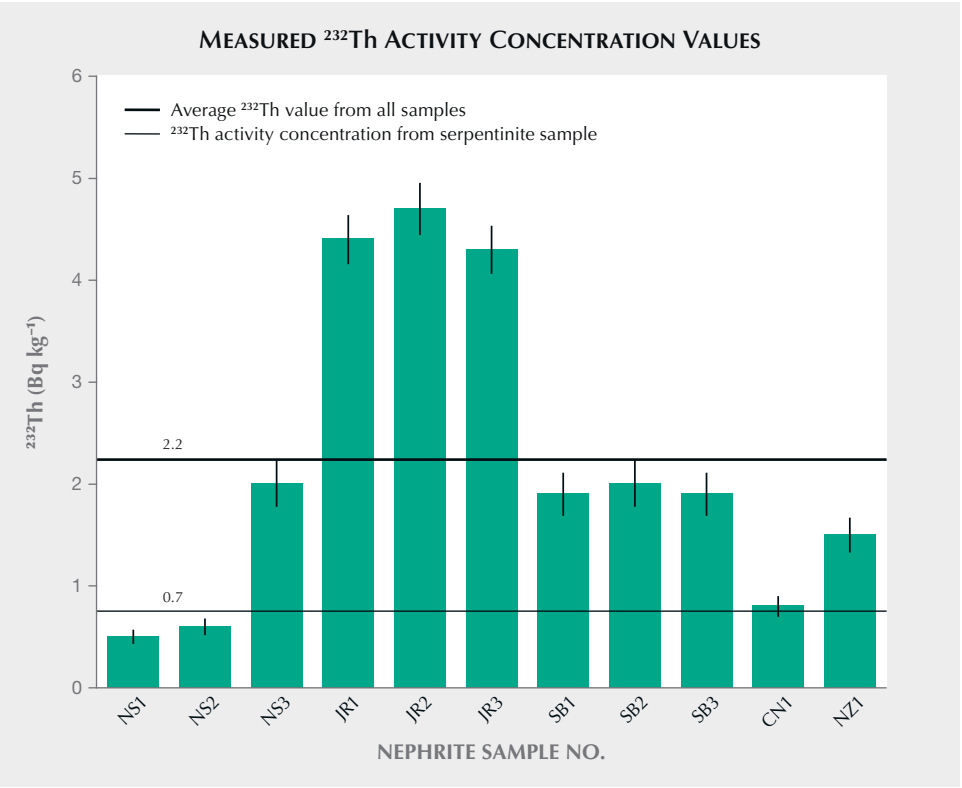

Figure 5. Measured ^{232}Th activity concentration values. The thick horizontal line represents the average ^{232}Th values from all samples. The thin horizontal line represents the ^{232}Th activity concentration for the serpentinite sample (SRN). The thin vertical lines are error bars.

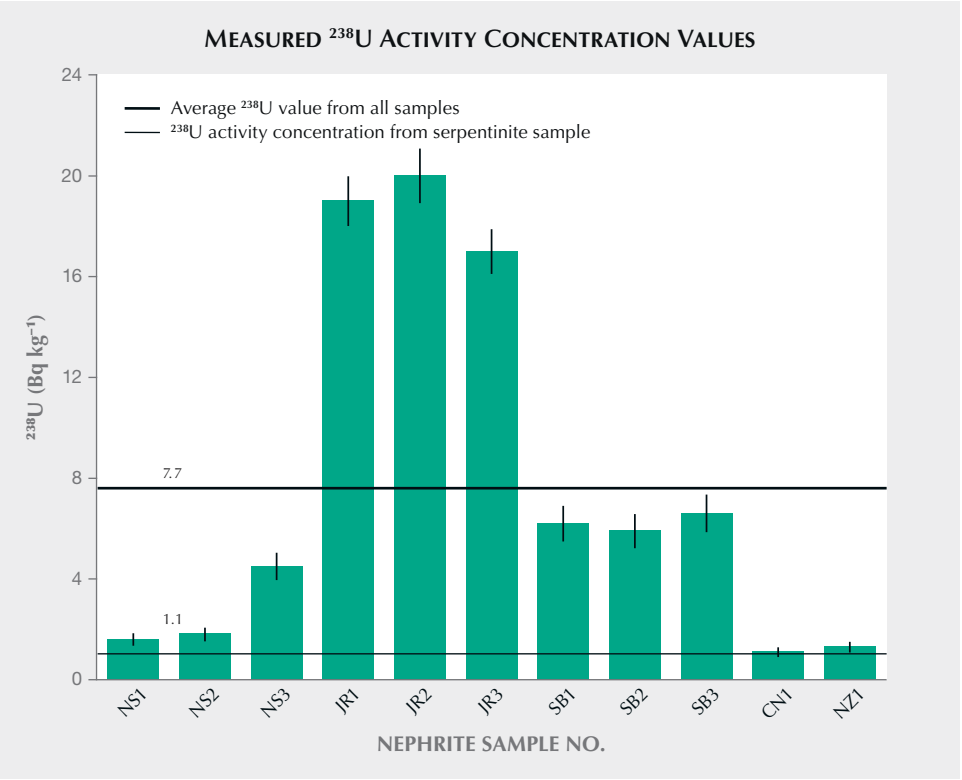

Figure 6. Measured ^{238}U activity concentration values. The thick horizontal line represents the average ^{238}U value from all samples in this study. The thin horizontal line represents the ^{238}U activity concentration for the serpentinite sample (SRN). The thin vertical lines are error bars.

Plewa, 1992). Typical granites give values ranging from 900–1400 Bq kg^{-1}.

^{232}Th. As seen in table 1 and figure 5, the nephrite from Jordanów had the highest activity concentration values associated with ^{232}Th series isotopes. Values of 4.3, 4.4, and 4.7 Bq kg^{-1} yielded an average ^{232}Th activity concentration of 4.5 Bq kg^{-1}. The samples from Siberia and Nasławice (NS3) showed the second-highest values at about 2 Bq kg^{-1}. Sample NZ1 had a similar value of 1.5 Bq kg^{-1}. The samples from Nasławice (NS1 and NS2) gave the lowest ^{232}Th activity concentrations of 0.5–0.6 Bq kg^{-1}. Sample CN1 also had a low value of 0.8 Bq kg^{-1}. All samples combined gave an average ^{232}Th activity concentration of 2.2 Bq kg^{-1} (figure 5). All measured activity concentrations exceeded values reported for ultrabasic rocks of an order of 10^{-2} Bq kg^{-1} (Van Schmus, 1995). The ^{232}Th activity concentration for all samples except NS1 and NS2 exceeded that measured from SRN (0.7 Bq kg^{-1}). Activity concentrations for nephrite samples analyzed fell below the average estimated for gabbros from Lower Silesia (6.4 Bq kg^{-1}) and well below that previously estimated for granites, which give ^{232}Th activity concentrations ranging from 50–200 Bq kg^{-1} with an average of 70 Bq kg^{-1} (Eisenbud and Gesell, 1997).

^{238}U. Table 1 and figure 6 show that the nephrite samples from Jordanów had the highest average activity concentration associated with ^{238}U series isotopes (19 Bq kg^{-1}). Samples from Siberia gave the second-highest average value at 6.3 Bq kg^{-1}. Samples CN1 and NZ1 showed the lowest ^{238}U activity concentrations of 1.2 and 1.3 Bq kg^{-1}, respectively. As with their ^{40}K and ^{232}Th values, the NS1 and NS2 nephrites from Nasławice gave lower ^{238}U activity concentration values (1.6 and 1.8 Bq kg^{-1}) relative to sample NS3 (4.5 Bq kg^{-1}). All samples had higher ^{238}U activity concentration values than those measured from ultrabasic rocks (~0.1 Bq kg^{-1}; Van Schmus, 1995) and from the serpentinite sample SRN (1.1 Bq kg^{-1}). As shown in figure 6, the ^{238}U activity concentration average of 7.7 Bq kg^{-1} measured for all nephrite samples exceeded the average of 4.1 Bq kg^{-1} measured from gabbros (Plewa and Plewa, 1992). This relatively high value arises from the significantly higher ^{232}Th activity concentration measured in the nephrite samples from Jordanów. The calculated mean for the ortho-nephrites analyzed fell below the previously reported average values for granite of 40 Bq kg^{-1} (Eisenbud and Gesell, 1997).

This study also compared ^{40}K, ^{232}Th, and ^{238}U activity concentrations from ortho-nephrite with those previously measured from marbles using the same

technique. Calcite marbles from the Sławniowice quarry (Lower Silesia, Poland) and Alpine marbles from the vicinity of Aussois (France) gave average ^{232}Th activity concentration values of 2.4 Bq kg^{-1} (Malczewski and Żaba, 2012; Moska, 2019). This approximated average value for ^{232}Th (2.2 Bq kg^{-1}) was measured from the ortho-nephrites analyzed. The ^{238}U activity concentrations in calcite marbles ranged from 16–23 Bq kg^{-1}. Nephrite ^{238}U activity concentrations ranged from 2 to 20 Bq kg^{-1} with an average value of ~8 Bq kg^{-1}. The measured ^{40}K activity concentrations for calcite marbles ranged from 12–80 Bq kg^{-1}, while that for nephrite ranged from 1.2–27 Bq kg^{-1} with an average of 9 Bq kg^{-1}. The dolomite marbles collected from the Sławniowice mine gave ^{40}K activity concentrations of 122 Bq kg^{-1} and ^{232}Th activity concentrations of 5 Bq kg^{-1}. These exceeded values measured from calcite marbles, but the two rock types exhibited similar ^{238}U concentrations of ~13 Bq kg^{-1}. The ortho-nephrites analyzed gave comparable ^{232}Th and ^{238}U activity concentration values but lower ^{40}K activity concentration values relative to those of calcite and dolomite marbles. Based on their analyses using an HPGe detector, Fares et al. (2011) reported a higher average ^{238}U activity concentration of 57 Bq kg^{-1} for commercial marbles from Egypt.

Rodingite. As noted earlier, the rodingite samples associated with the Nasławice and Jordanów nephrite deposits classify as boninite (RN3) and plagiogranite rodingite (RN1 and RN2). As shown in table 1 and figure 7, sample RN1 gave the highest ^{238}U and ^{232}Th activity concentrations of 292 and 130 Bq kg^{-1}, respectively. These values significantly exceed the activity concentrations of all examined nephrites and activity concentrations of typical granites of 40 and 70 Bq kg^{-1} for ^{238}U and ^{232}Th, respectively (Eisenbud and Gesell, 1997). Sample RN2 also exhibited high uranium activity concentration but lower thorium-related activity concentration relative to sample RN1. The high ^{238}U and ^{232}Th activity concentration values in RN1 and RN2 rodingite samples likely reflect the presence of accessory zircon, thorianite, and uraninite (Szełęg, 2006). As expected, sample RN3, which was collected from a body in direct contact with the nephrite-bearing zone, exhibited significantly lower ^{238}U and ^{232}Th activity concentrations than samples RN1 and RN2. Activity concentrations

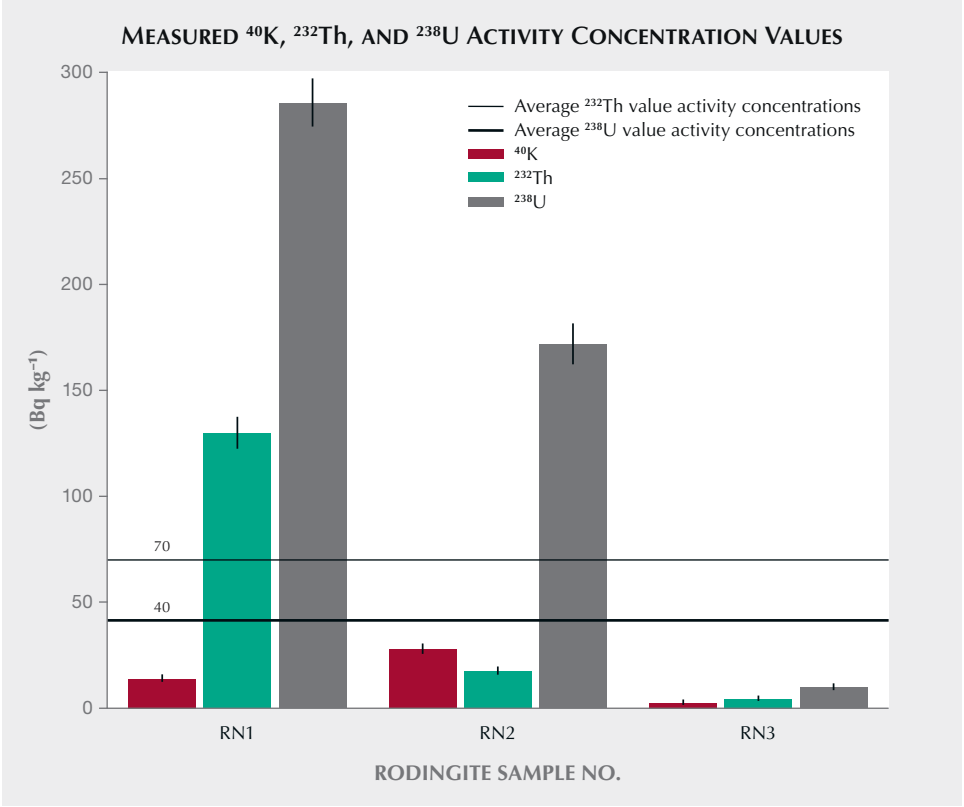

Figure 7. Measured ^{40}K, ^{232}Th, and ^{238}U activity concentration values for rodingite. The thin and thick horizontal lines respectively show the average ^{232}Th and ^{238}U activity concentrations in typical granites (Eisenbud and Gesell, 1997). The thin vertical lines are error bars.

measured from RN3 for ^{238}U (10 Bq kg^{-1}) and ^{232}Th (5 Bq kg^{-1}) exceeded those observed in ortho-nephrite samples from Nasławice, Siberia, British Columbia, and South Island but resembled those measured from the Jordanów samples. The rodingite samples exhibited relatively low ^{40}K activity concentrations with a mean value of 15 Bq kg^{-1}, which exceeded the mean value of 9.1 Bq kg^{-1} measured from the nephrite samples. As with ^{238}U and ^{232}Th activity concentrations, sample RN3 gave the lowest ^{40}K activity concentration of 3 Bq kg^{-1}. Samples RN1 and RN2 gave higher activity concentrations of 14 and 28 Bq kg^{-1}. These resembled values measured from the Jordanów nephrite samples and from CN1.

Comparison of K, Th, and U Concentrations with Previous Data. Concentrations estimated for potassium (wt.%), thorium (ppm), and uranium (ppm) showed similar trends among the samples as those observed for the ^{40}K, ^{232}Th, and ^{238}U activity concentration values. Nephrite potassium concentrations varied from 0.004 wt.% for sample NS2 to 0.087 wt.% for sample CN1, and the samples overall gave a mean value of 0.03%. Concentrations estimated for potassium, thorium, and uranium generally resembled the few previously obtained results for ortho-nephrite from the same locations. The nephrite samples from Nasławice in particular showed similar potassium concentrations. Łoboś et al. (2008) report average potassium concentrations of 0.004, 0.008, and 0.016 wt.% for three types of nephrite based on electron microscope analysis. These values correspond to ^{40}K activity concentrations of approximately 1.2, 2.5, and 5.0 Bq kg^{-1} and thus agree very well with activity concentrations measured from samples NS1, NS2, and NS3 by gamma-ray spectrometry (table 1). Prompt gamma neutron activation energy analysis (PGAA) indicated a bulk-rock potassium concentration of about 0.016 wt.% for the Jordanów nephrite sample. This value corresponds to a ^{40}K activity concentration of less than 5 Bq kg^{-1} (Gil et al., 2015). The concentration value and associated ^{40}K activity concentration fell below values obtained by this study for the three samples from Jordanów, which gave an average potassium concentration of 0.050 wt.% and an average ^{40}K activity concentration of 15 Bq kg^{-1} (table 1). Extensive studies by Leaming (1978) and Nichol (2000) report an average potassium concentration of 0.038 wt.% and a corresponding ^{40}K activity concentration of 12 Bq kg^{-1} for Canadian nephrite from British Columbia. Gamma-ray measurements (table 1) of sample CN1 indicate a higher but comparable ^{40}K activity concentration value of 27 Bq kg^{-1} (0.087 wt.%). Grapes and Yun (2010) report average potassium concentrations for South Island nephrite of 0.012 wt.% based on electron microprobe analysis. These correspond to a ^{40}K activity concentration of 3.8 Bq kg^{-1} and fall within the measurement uncertainty of potassium values obtained for sample NZ1 (4.2 Bq kg^{-1} and 0.014 wt.%). The above-mentioned literature sources provide no data on thorium and uranium concentrations.

Ortho-nephrite samples from the East Sayan area exhibit relatively large differences in potassium, thorium, and uranium concentrations. Inductively coupled plasma–mass spectrometry (ICP-MS) analysis gave average potassium concentrations of 0.05 wt.% (16 Bq kg^{-1} of ^{40}K) for samples from the area (Burtseva et al., 2015). This value exceeds the average value of 0.016 wt.% (6 Bq kg^{-1} of ^{40}K) obtained for samples SB1, SB2, and SB3. Burtseva et al. (2015) reported average thorium and uranium concentrations for nine samples of 0.06 ppm (~0.3 Bq kg^{-1} for thorium) and 0.05 ppm (~0.6 Bq kg^{-1} for uranium). The present study obtained mean thorium and uranium activity concentrations of 1.9 and 6.2 Bq kg^{-1}, corresponding to concentrations of 0.48 and 0.51 ppm from East Sayan nephrite (table 1).

Comparison of K, Th, and U Concentrations Measured from Para-Nephrite. Luo et al. (2015) present detailed laser ablation–inductively coupled–mass spectrometry (LA-ICP-MS) trace element data for 138 samples collected directly from eight major dolomite-related nephrite deposits in East Asia. Figure 8 compares mean potassium, thorium, and uranium concentrations reported in Luo et al. (2015) with results from ortho-nephrite samples reported in this study. As seen in figure 8A, the ortho-nephrites exhibit an average potassium concentration of 0.03 wt.%, whereas the para-nephrites from East Asia exhibit an average potassium concentration of 0.07 wt.% (22 Bq kg^{-1}) with standard deviations of 0.02 and 0.04%, respectively. Nichol (2000) reports a mean potassium concentration of 0.1 ± 0.02 wt.% for para-nephrite samples from southern Australia. This corresponds to a ^{40}K activity concentration of approximately 30 Bq kg^{-1}, a value that resembles that measured for sample CN1, which gave the highest ^{40}K activity concentration among the ortho-nephrite samples (table 1). Similarly, dolomite-related nephrite from Val Malenco (Italy) had a mean potassium concentration of 0.04 ± 0.004 wt.%, which slightly exceeded the average values

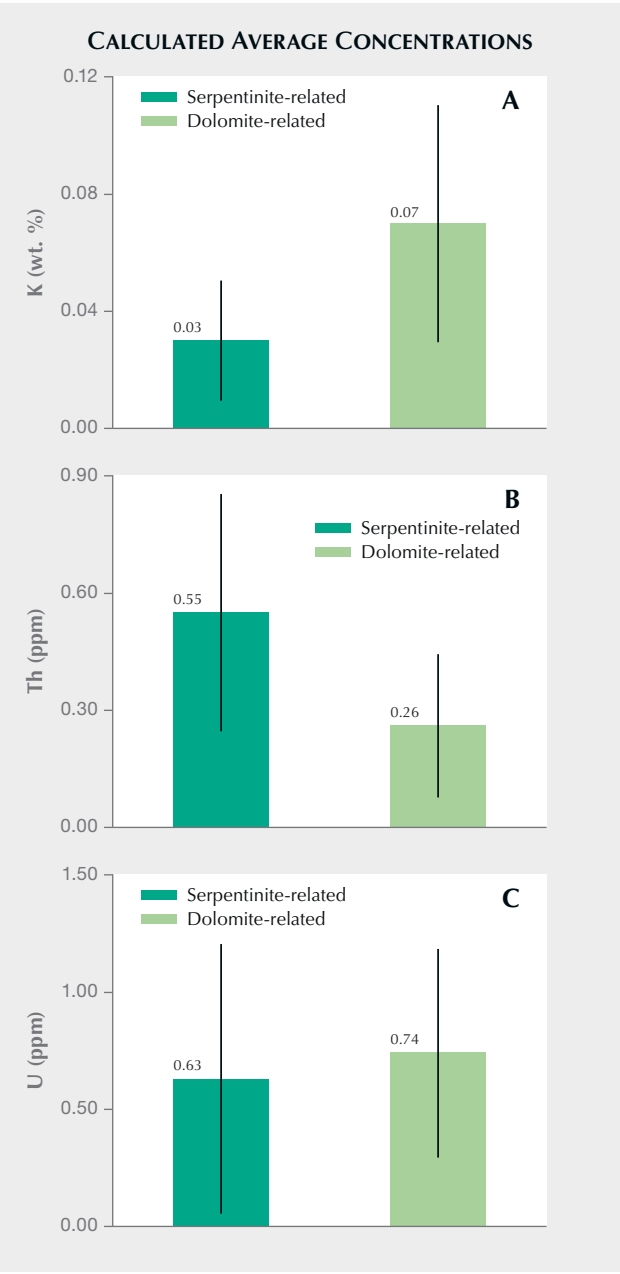

Figure 8. Comparison of calculated average concentrations of potassium (wt.%), thorium (ppm), and uranium (ppm) in ortho-nephrites (serpentine-related, darker green bar) analyzed in this study and from para-nephrite (dolomite-related, lighter green bar) data reported by Luo et al. (2015). The thin vertical lines are error bars.

obtained for ortho-nephrites reported here. A concentration of 0.04 wt.% potassium corresponds to a ^{40}K activity concentration of about 12 Bq kg^{-1}. This estimate resembles values measured for the Jordanów nephrites (table 1). Results also show that the mean potassium concentration calculated from ortho-nephrite ^{40}K activity concentration generally falls below that measured for para-nephrite (figure 8A). However, potassium concentrations often overlap for both types of nephrite. Serpentinite-related nephrites gave an estimated average thorium concentration of 0.55 ± 0.30 ppm, which exceeds that estimated for para-nephrite (0.26 ± 0.18 ppm or 1.1 ± 0.7 Bq kg^{-1}) by a factor of two (figure 8B). The relatively large dispersion of thorium concentrations for both types of nephrite means that value ranges partially overlap. Excluding the Jordanów samples with the highest thorium concentrations gives a calculated mean of 0.35 for the remaining serpentinite-related nephrites. This value still exceeds the values estimated for dolomite-related nephrite. As shown in figure 8C, serpentinite-related nephrites gave an average U concentration of 0.63 ± 0.57 ppm, while dolomite-related nephrites had an average uranium concentration of 0.74 ± 0.44 ppm (9.1 ± 5.4 Bq kg^{-1}). Ortho-nephrite and para-nephrite showed very similar average uranium concentrations, but samples from different nephrite deposit locations give relatively variegated values. In summary, the relatively large standard deviations associated with calculated mean potassium, thorium, and uranium concentrations suggest that these parameters alone would not be enough to clearly distinguish ortho-nephrite from para-nephrite but may serve as approximate indicators of host rock type, especially in terms of their potassium and thorium parameters.

Correlations Between Th and U Concentrations. As seen in figure 9, ^{232}Th and ^{238}U concentrations correlate strongly in ortho-nephrites analyzed and give a correlation coefficient of 0.98. A fitted line shows samples NS1 and NZ1 deviate slightly from this trend. Figure 9 shows that Jordanów samples (JR1–JR3) form a distinct data cluster with uranium concentrations ranging from 1.3 to 1.7 ppm and thorium concentrations from 1.0 to 1.2 ppm. All other ortho-nephrite samples range from about 0.1 to 0.6 ppm in terms of both uranium and thorium concentrations. A gap of 0.7 to 1.3 ppm for uranium and 0.6 to 1.0 for thorium thus exists between the Jordanów samples and others. Excluding the CN1 sample, other samples also show strong K-Th and K-U correlations (table 1).

The dolomite-related nephrites from deposits in East Asia studied by Luo et al. (2015) showed weaker correlations between average thorium and uranium concentrations. These gave average thorium concen-

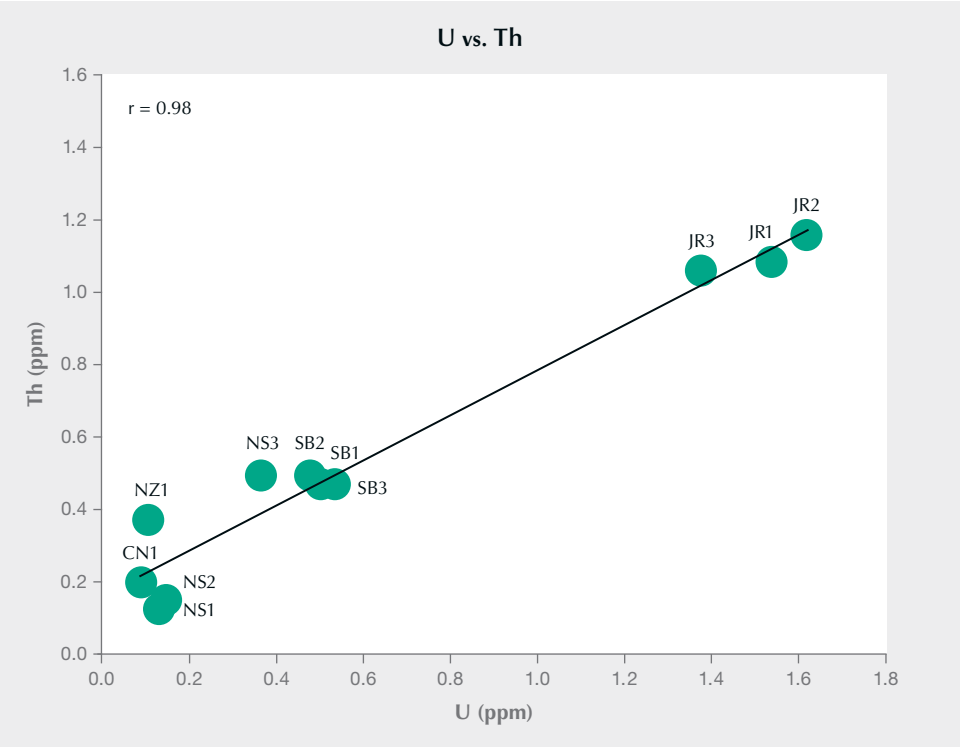

Figure 9. Correlation between thorium (ppm) and uranium (ppm) for ortho-nephrites analyzed in this study. The solid line represents the linear fit of Th (ppm) = 0.16 + 0.62 × U (ppm), with a correlation coefficient of r = 0.98.

trations of 0.07 to 0.70 ppm and uranium concentrations from 0.2 to 1.4 ppm. Data from these para-nephrites show a high degree of visible scatter, and linear regression gives a correlation coefficient of 0.42 (figure 10). The weaker correlation between thorium and uranium concentrations for para-nephrite (figure 10) compared to that observed for ortho-nephrite (figure 9) most likely arises from greater differentiation of

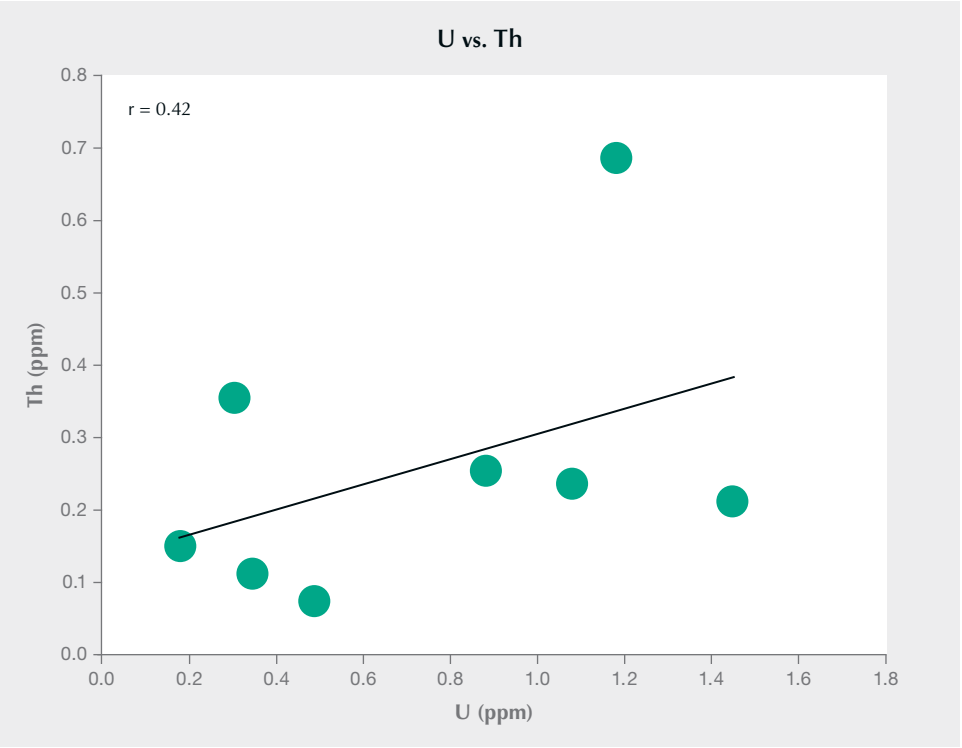

Figure 10. Correlation between thorium (ppm) and uranium (ppm) for para-nephrites based on data reported in table 2 of Luo et al. (2015). The solid line represents a linear fit of Th (ppm) = 0.13 + 0.17 × U (ppm), with a correlation coefficient of r = 0.42.

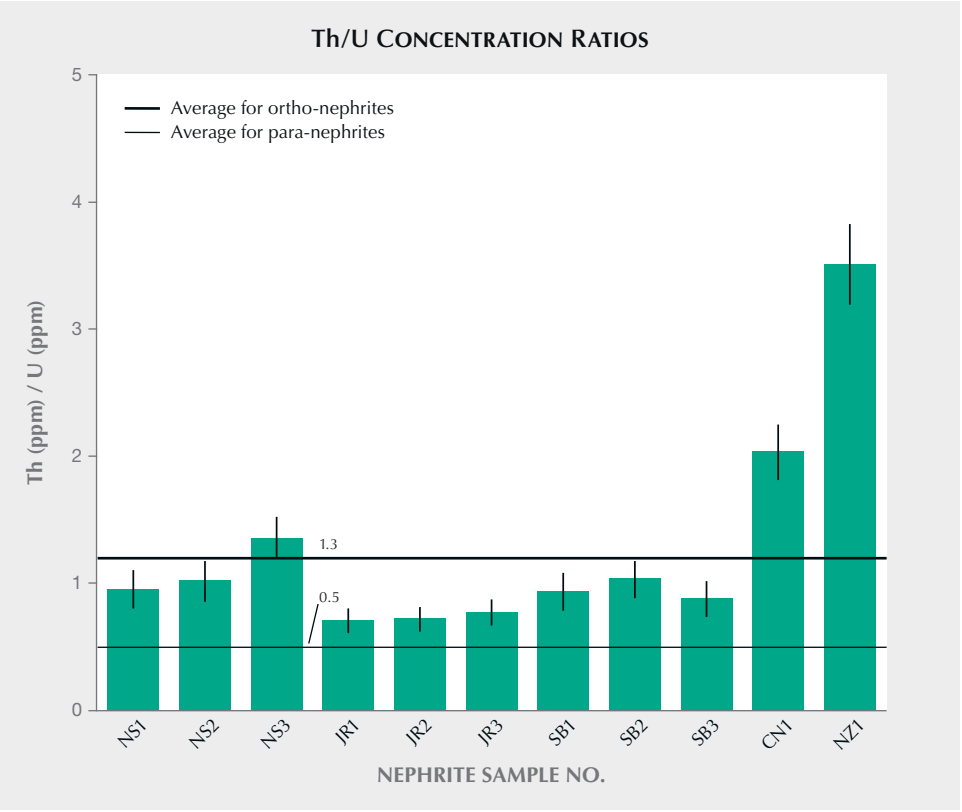

Figure 11. Concentration ratios of Th/U. The thick horizontal line shows the average for ortho-nephrites in the present study. The thin horizontal line shows the average for para-nephrites based on data reported by Luo et al. (2015). The thin vertical lines are error bars.

thorium and uranium concentrations in dolomites (and carbonates in general), which are the host rocks for para-nephrite.

Th/U Concentration Ratios. As shown in figure 11, Th/U ratios for the serpentinite-related nephrites vary from 0.70 to 3.51 with an average value of 1.30. The average Th/U concentration ratios were 1.11 ± 0.12, 0.73 ± 0.02, and 0.95 ± 0.05 for nephrite from Nasławice, Jordanów, and Siberia, respectively. Nephrite from these locations can be differentiated within standard deviations based on their Th/U ratio (figure 11). Despite its higher thorium and uranium concentrations, sample NS3 gave a Th/U ratio similar to that of samples NS1 and NS2. Samples CN1 and NZ1 gave relatively higher Th/U ratios of 2.03 ± 0.14 and 3.51 ± 0.25, respectively.

The data presented by Luo et al. (2015) indicates a calculated mean Th/U value of 0.5 for dolomite-related nephrite. This value falls below the value of 1.3 estimated for serpentinite-related nephrite by the present study (figure 11). The calculated values of 1.3 and 0.5 for serpentinite- and dolomite-related nephrite (respectively) resemble Th/U concentration ratios in the host rocks. Serpentinites and their peridotite protoliths both exhibit a Th/U ratio of approximately 2 (Van Schmus, 1995; Pasquale et al., 2001). As listed in table 1, the serpentinite from Nasławice (SN1) gave a ratio of 1.9, which approaches the mean value estimated for ortho-nephrite. Previous studies of dolomite and dolomite marble using gamma-ray spectrometry show that the average Th/U ratio for these rocks is about 0.5 (Chiozzi et al., 2002; Malczewski et al., 2005; Malczewski and Żaba, 2012; Moska, 2019). Generally, carbonate rocks have a mean Th/U value of 0.8 (Van Schmus, 1995). Again, the average value of the Th/U ratio calculated for the para-nephrites based on the results obtained by Luo et al. (2015) agrees well with those reported for carbonate rocks and especially dolomites.

CONCLUSIONS

This study reports gamma-ray spectrometric analysis of serpentinite-related nephrite samples from several well-known global localities. Measurements indicate very low ^{40}K, ^{232}Th, and ^{238}U activity concentrations that pose no radiological risk. Measured activity concentrations fell below values reported in the literature for acid igneous rocks. By contrast, the mean ^{40}K, ^{232}Th, and ^{238}U activity concentration values exceeded average values reported in literature sources for ultrabasic rocks and, to a lesser ex-

Figure 12. This 90 × 20 mm nephrite carving is from the Kutcho Jade mine in northwest British Columbia, Canada. Photo by Robert Weldon; courtesy of Jade West Group.

tent, for serpentinites. Compared to gabbroic rocks from Lower Silesia (Poland), the ortho-nephrites exhibited lower ^{40}K and ^{232}Th activity concentrations and slightly higher ^{238}U activity concentrations. The

measured serpentinite-related nephrites were characterized by extremely low average values of radiological hazard indices I and H_{ex} of 0.04 and 0.03, with the upper levels of both indices equal to unity. Calculated thorium (ppm) and uranium (ppm) concentrations strongly correlate. Nephrite from Nasławice, Jordanów, and Siberia show distinct Th/U ratios, indicating that this parameter may distinguish material from these respective localities. Our results suggest that relative to para-nephrite, ortho-nephrite (figure 12) exhibits lower potassium concentration values and higher thorium concentrations. Both types of nephrite jade exhibit similar uranium concentrations.

ABOUT THE AUTHORS

Dr. Malczewski is a nuclear physicist and assistant professor at the Institute of Earth Sciences of the University of Silesia (Poland), specializing in the field of natural and anthropogenic radioactivity in the geosphere and researching metamict minerals as natural analogues for understanding the storage of high-level nuclear waste. Professor Sachanbiński, who specializes in the physics of minerals, gemology, and mineralogy, is an emeritus professor at the University of Wrocław and teaches at the College of Arts and Management in Wrocław. Dr. Dziurowicz is a geologist, geophysicist, and assistant professor at the Institute of Earth Sciences of the University of Silesia, specializing in natural and anthropogenic environmental radioactivity.

ACKNOWLEDGMENTS

This work was partially supported by the National Science Centre of Poland through grant no. 2018/29/B/ST10/01495 and the research program at the Institute of Earth Sciences, University of Silesia, ZB-14-2020. We thank the Mineralogical Museum at the Institute of Earth Sciences, University of Silesia, and Stanisław Madej for the New Zealand jade sample and rodingite samples used in this research. The authors would like to thank Sandra Malczewska for the digital processing of photos according to publication requirements.

REFERENCES

Adamo I., Bocchio R. (2013) Nephrite jade from Val Malenco, Italy: Review and update. *G&G*, Vol. 49, No. 2, pp. 98–106, http://dx.doi.org/10.5741/GEMS.49.2.98

Bell J.M., de Courcey Clarke E., Marshall P. (1911) Geology of the Dun Mountain Subdivision. *New Zealand Geological Survey*, Bulletin No. 12, pp. 31–35.

Burtseva M.V., Ripp G.S., Posokhov V.F., Murzintseva A.E. (2015) Nephrites of East Siberia: Geochemical feature and problems of genesis. *Russian Geology and Geophysics*, Vol. 56, No. 3, pp. 402–410, http://dx.doi.org/10.1016/j.rgg.2015.02.003

Chiozzi P., Pasquale V., Verdoya M. (2002) Naturally occurring radioactivity at the Alps-Apennines transition. *Radiation Measurements*, Vol. 35, No. 2, pp. 147–154, http://dx.doi.org/10.1016/S1350-4487(01)00288-8

Cooper A.F. (1995) Nephrite and metagabbro in the Haast Schist at Muddy Creek, northwest Otago, New Zealand. *New Zealand Journal of Geology and Geophysics*, Vol. 38, No. 3, pp. 325–332, http://dx.doi.org/10.1080/00288306.1995.9514660

Douglas J.G. (2005) A review of some recent research on early Chinese jades. In *Scientific Examination of Art: Modern Techniques in Conservation and Analysis*. National Academies Press, Washington, DC, pp. 206–214.

Dubińska E., Gunia P. (1997) The Sudetic ophiolite: Current view on its geodynamic model. *Geological Quarterly*, Vol. 41, No. 1, pp. 1–20.

Dubińska E., Bylina P., Kozłowski A., Dörr W., Nejbert K., Schastok J., Kulicki C. (2004) U-Pb dating of serpentinization: Hydrothermal zircon from a metasomatic rodingite shell (Sudetic ophiolite, SW Poland). *Chemical Geology*, Vol. 203, No. 3-4, pp. 183–203, http://dx.doi.org/10.1016/j.chemgeo.2003.10.005

Eisenbud M., Gesell T. (1997) *Environmental Radioactivity Concentration from Natural, Industrial and Military Sources*. Academic Press, San Diego.

European Atomic Energy Community (2013) Council Directive EU 2013/59/Euratom. Laying down basic safety standards for protection against the dangers arising from exposure to ionising radiation.

Fares S., Yassene A.A.M., Ashour A., Abu-Assy M.K., Abd El-Rahman M. (2011) Natural radioactivity and the resulting radiation doses in some kinds of commercially marble collected from different quarries and factories in Egypt. *Natural Science*, Vol. 3, No. 10, pp. 895–905, http://dx.doi.org/10.4236/ns.2011.310115

Gao K., Fang T., Lu T., Lan Y., Zhang Y., Wang Y., Chang Y. (2020) Hydrogen and oxygen stable isotope ratios of dolomite-related nephrite: Relevance for its geographic origin and geological significance. *G&G*, Vol. 56, No. 2, pp. 266–280, http://dx.doi.org/10.5741/GEMS.56.2.266

Gil G. (2013) Petrographic and microprobe study of nephrites from Lower Silesia (SW Poland). *Geological Quarterly*, Vol. 57, No. 3, pp. 395–404, http://dx.doi.org/10.7306/gq.1101

Gil G., Barnes J.D., Boschi C., Gunia P., Szakmány G., Bendö Z., Raczyński P., Péterdi B. (2015) Origin of serpentinite-related nephrite from Jordanów and adjacent areas (SW Poland) and its comparison with selected nephrite occurrences. *Geological Quarterly*, Vol. 59, No. 3, pp. 457–472, http://dx.doi.org/10.7306/gq.1228

Gil G., Bagiński B., Gunia P., Madej S., Sachanbiński M., Jokubauskas P., Belka Z. (2020) Comparative Fe and Sr isotope study of nephrite deposits hosted in dolomitic marbles and serpentinites from the Sudetes, SW Poland: Implications for Fe-As-Au-bearing skarn formation and post-obduction evolution of the oceanic lithosphere. *Ore Geology Reviews*, Vol. 118, article no. 103335, http://dx.doi.org/10.1016/j.oregeorev.2020.103335

Grapes R.H., Yun S.T. (2010) Geochemistry of a New Zealand nephrite weathering rind. *New Zealand Journal of Geology and Geophysics*, Vol. 53, No. 4, pp. 413–426, http://dx.doi.org/10.1080/00288306.2010.514929

Hatzipanagiotou K., Tsikouras B. (2001) Rodingite formation from

diorite in the Samothraki ophiolite, NE Aegean, Greece. *Geological Journal*, Vol. 36, No. 2, pp. 93–109, http://dx.doi.org/10.1002/gj.887
Heflik W., Natkaniec-Nowak L., Dumańska-Słowik A. (2014) Rodingite from Nasławice and the other occurrences of these rocks in Lower Silesia (SW Poland). *Geological Quarterly*, Vol. 58, No. 1, pp. 31–40.
Hobbs J.M. (1982) The jade enigma. *G&G*, Vol. 18, No. 1, pp. 3–19, http://dx.doi.org/10.5741/GEMS.18.1.3
International Atomic Energy Agency (2003) IAEA-TECDOC-1363: Guidelines for radioelement mapping using gamma ray spectrometry data. Vienna.
Ireland T.R., Reay A., Cooper A.F. (1984) The Pounamu ultramafic belt in the Dietrich Range, Westland, New Zealand. *New Zealand Journal of Geology and Geophysics*, Vol. 27, No. 3, pp. 247–256.
Kobayashi S., Kaneda H. (2010) Rodingite with Ti- and Cr-rich vesuvianite from the Sartuohai chromium deposit, Xinjiang, China. *Journal of Mineralogical and Petrological Sciences*, Vol. 105, No. 3, pp. 112–122, http://dx.doi.org/10.2465/jmps.081224
Leaming S.F. (1978) *Jade in Canada*. Geological Survey of Canada, Paper 78-19. Energy, Mines & Resources, Canada, 59 pp.
Łoboś K., Sachanbiński M., Pawlik T. (2008) Nephrite from Nasławice in Lower Silesia (SW Poland). *Przegląd Geologiczny*, Vol. 56, No. 11, pp. 991–999 (in Polish with English abstract).
Luo Z., Yang M., Shen A.H. (2015) Origin determination of dolomite-related white nephrite through iterative-binary linear discriminant analysis. *G&G*, Vol. 51, No. 3, pp. 300–311, http://dx.doi.org/10.5741/GEMS.51.3.300
Makepeace K., Simandl G.J. (2001) Jade (nephrite) in British Columbia, Canada. *Program and Extended Abstracts for 37th Forum on the Geology of. Industrial Minerals* 37, pp. 209– 210.
Malczewski D., Żaba J. (2012) Natural radioactivity in rocks of the Modane-Aussois region (SE France). *Journal of Radioanalytical and Nuclear Chemistry*, Vol. 292, No. 1, pp. 123–130, http://dx.doi.org/10.1007/s10967-011-1428-9
Malczewski D., Teper L., Lizurek G., Dorda J. (2005) In situ gamma-ray spectroscopy in common rock raw materials mined in Kraków vicinity, Poland. In *Naturally Occurring Radioactive Materials (NORM IV)*: *Proceedings of an International Conference Held in Szczyrk, Poland, 17–21 May 2004*. IAEA-TECDOC-1472. International Atomic Energy Agency, Lanham, Maryland, pp. 368–376.
Malczewski D., Dziurowicz M., Krzykawski T., Grabias A. (2018a) Spectroscopic characterization and thermal recrystallization study of an unknown metamict phrase from Tuften Quarry, Southern Norway. *The Canadian Mineralogist*, Vol. 56, No. 4, pp. 365– 373, http://dx.doi.org/10.3749/canmin.1800015
Malczewski D., Dziurowicz M., Krzykawski T., Stryjewski A. (2018b) ^{222}Rn and ^{220}Rn emanations from zircon crystals as a function of absorbed alpha-doses. *The Canadian Mineralogist*, Vol. 56, No. 4, pp. 451–462, http://dx.doi.org/10.3749/canmin.1700089
Moska A. (2019) Natural and anthropogenic radioactivity of the Opava Mountains and their western foreland. PhD thesis. University of Silesia, Katowice, Poland (in Polish with English abstract).
Nichol D. (2000) Two contrasting nephrite jade types. *Journal of Gemmology*, Vol 27, No. 4, pp. 193–200.
O'Brien J.P., Rodgers K.A. (1973) Xonitlite and rodingites from Wairere, New Zealand. *Mineralogical Magazine*, Vol. 39, No. 302, pp. 233–240.
Pasquale V., Verdoya M., Chiozzi P. (2001) Radioactive heat generation and its thermal effects in the Alps-Apennines boundary zone. *Tectonophysics*, Vol. 331, No. 3, pp. 269–283, http://dx.doi.org/10.1016/S0040-1951(00)00294-8
Plewa M., Plewa S. (1992) *Petrophysics*. Geological Publishing House, Warsaw, 326 pp. (in Polish).
Prichystal A. (2013) *Lithic Raw Materials in Prehistoric Times of Eastern Central Europe*. Masaryk University, Brno, Czech Republic.
Suturin A.N., Zamaletdinov R.S., Letnikov F.A., Sekerin A.P. Burmakina G.V., Suturina T.A., Platonov A.N., Belitchenko V.P., Vokhmentser A.Y. (1980) Mineralogy and genesis of nephrites in the USSR. In Sidorenko, Eds., *Gem Minerals: Proceeding of the XI General Meeting of IMA*, Novosibirsk, September 4–10, 1978 (in Russian).
Szełęg E. (2006) Crystalochemistry of titanite from Lower Silesian. PhD thesis. University of Silesia, Katowice, Poland (in Polish).
UNSCEAR (2000) Sources and Effects of Ionizing Radiation: Vol I. United Nations Scientific Committee on the Effects of Atomic Radiation. UNSCEAR 2000 Report to the General Assembly, with Scientific Annexes. United Nations, New York.
Van Schmus W.R. (1995) Natural radioactivity of the crust and the mantle. In T.J. Ahrens, Ed., *Global Earth Physics: A Handbook of Physical Constants*. AGU Reference Shelf I, American Geophysical Union, Washington, DC, pp. 283–291.
Wang R. (2011) Progress review of the scientific study of Chinese ancient jade. *Archaeometry*, Vol. 53, No. 4, pp. 674–692, http://dx.doi.org/10.1111/j.1475-4754.2010.00564.x
Wilkins C.J., Tennant W.C., Williamson B.E., McCammon C.A. (2003) Spectroscopic and related evidence on the coloring and constitution of New Zealand jade. *American Mineralogist*, Vol. 88, No. 8-9, pp. 1336–1344, http://dx.doi.org/10.2138/am-2003-8-917
Yui T.F., Kwon S.T. (2002) Origin of a dolomite-related jade deposit at Chumcheon, Korea. *Economic Geology*, Vol. 97, No. 3, pp. 593–601, http://dx.doi.org/10.2113/gsecongeo.97.3.593
Żaba J. (2006) *Illustrated Dictionary of Rocks and Minerals*. Videograf II Ltd., Katowice, Poland (in Polish).